Mon. Not. R. Astron. Soc. **311**, 23–36 (2000)

Ionization, shocks and evolution of the emission-line gas of distant 3CR radio galaxies

P. N. Best,[1]★ H. J. A. Röttgering[1] and M. S. Longair[2]
[1]*Sterrewacht Leiden, Postbus 9513, 2300 RA Leiden, the Netherlands*
[2]*Cavendish Astrophysics, Madingley Road, Cambridge, CB3 0HE*

Accepted 1999 July 27. Received 1999 July 22; in original form 1999 April 28

ABSTRACT

An analysis of the kinematics and ionization state of the emission-line gas of a sample of 14 3CR radio galaxies with redshifts $z \sim 1$ is carried out. The data used for these studies, deep long-slit spectroscopic exposures from the William Herschel Telescope, are presented in an accompanying paper. It is found that radio sources with small linear sizes ($\lesssim$150 kpc) have lower ionization states, higher emission-line fluxes and broader line widths than larger radio sources. An analysis of the low-redshift sample of Baum et al. demonstrates that radio galaxies at low redshift show similar evolution in their velocity structures and emission-line ratios from small to large radio sources.

The emission-line ratios of small radio sources are in agreement with theoretical shock ionization predictions, and their velocity profiles are distorted. Together with the other emission-line properties, this indicates that shocks associated with the radio source dominate the kinematics and ionization of the emission-line gas during the period that the radio source is expanding through the interstellar medium. Gas clouds are accelerated by the shocks, giving rise to the irregular velocity structures observed, whilst shock compression of emission-line gas clouds and the presence of the ionizing photons associated with the shocks combine to lower the ionization state of the emission-line gas. By contrast, in larger sources the shock fronts have passed well beyond the emission-line regions; the emission-line gas of these larger radio sources has much more settled kinematical properties, indicative of rotation, and emission-line ratios consistent with the dominant source of ionizing photons being the active galactic nucleus.

This strong evolution with radio size of the emission-line gas properties of powerful radio galaxies mirrors the radio size evolution seen in the nature of the optical–ultraviolet continuum emission of these sources, implying that the continuum alignment effect is likely to be related to the same radio source shocks.

Key words: shock waves – galaxies: active – galaxies: ISM – radio continuum: galaxies.

1 INTRODUCTION

Powerful high-redshift ($z \gtrsim 1$) radio galaxies display a number of remarkable characteristics. Their near-infrared emission shows them to be amongst the most massive galaxies known in the early Universe and to have radial light profiles following de Vaucouleurs' law, indicating that they are fully formed giant elliptical galaxies (Best, Longair & Röttgering 1998). At optical and rest frame ultraviolet (UV) wavelengths, however, the galaxies have very irregular morphologies, frequently showing a strong excess of emission aligned along the axis of the radio source (McCarthy et al. 1987; Chambers, Miley & van Breugel 1987). Their emission-line properties are equally spectacular; luminous emission-line regions surround the radio galaxies, extending for several tens of kiloparsecs or more (e.g. McCarthy, Spinrad & van Breugel 1995), with velocity shears up to a few hundred km s^{-1} and line widths as high as 1500 km s^{-1} (e.g. McCarthy, Baum & Spinrad 1996). The emission-line regions are characterized by high-ionization spectra including strong emission from species such as Ne V and C IV. The origin of this luminous emission-line gas, its kinematics and ionization, and their connection to the radio source phenomenon remain important astrophysical questions.

Over the past few years we have been carrying out a detailed investigation of a sample of 28 radio galaxies with redshifts $z \sim 1$ from the revised 3CR catalogue (Laing, Riley & Longair 1983),

★ E-mail: pbest@strw.leidenuniv.nl

using optical imaging with the *Hubble Space Telescope* (*HST*), high-resolution radio interferometry with the Very Large Array (VLA) and near-infrared imaging with the UK Infrared Telescope (UKIRT) (Longair, Best & Röttgering 1995; Best, Longair & Röttgering 1996, 1997; Best et al. 1998). Here, and in an accompanying paper (Best, Röttgering & Longair 1999; hereafter Paper I), results are presented from a deep spectroscopic campaign using the William Herschel Telescope (WHT) on 14 of these radio galaxies, to study in detail the emission-line gas. The reader is referred to Paper I for details of the sample selection, data reduction, the reduced one-dimensional spectra and tabulated line fluxes, and the distributions of the intensity, velocity and line width of the emission-line gas as a function of position along the slit for each galaxy.

The current paper is concerned with investigating the galaxy-to-galaxy variations in the ionization and kinematics of the emission-line gas, and comparing these variations with the radio and optical properties. The layout is as follows. In Section 2 the photoionization and shock ionization models are discussed and their predictions are compared with the observed emission-line ratios of the galaxies on an emission-line diagnostic diagram. The kinematics of the gas are studied in Section 3. In Section 4 the results are compared with those of a low-redshift sample of galaxies, and a scenario is proposed to explain the observed properties of the emission-line gas at low and high redshifts. The spectroscopic properties of the distant galaxies are compared to their optical properties, and the implications of these results for the continuum alignment effect are discussed. Conclusions are drawn in Section 5. Throughout the paper, values for the cosmological parameters of $\Omega = 1$ and $H_0 = 50\,\mathrm{km\,s^{-1}\,Mpc^{-1}}$ are assumed.

2 THE IONIZATION OF THE EXTENDED EMISSION-LINE REGIONS

Robinson et al. (1987) showed that for most low-redshift ($z \lesssim 0.1$) radio galaxies, the emission-line spectrum can be explained adequately if it is assumed that the gas is photoionized by a power-law emission source such as that provided by an active galactic nucleus (AGN). Baum, Heckman & van Breugel (1992) obtained similar results for a sample of radio galaxies out to redshift 0.2, although they noted that photoionization models could not reproduce [N II] 6584 / Hα ratios as high as were observed for some galaxies; they suggested that localized sources of heating and ionization, for example shocks or the UV continuum of surrounding hot gas (e.g. Heckman et al. 1989), may play a role in some radio sources. McCarthy (1993) constructed a composite spectrum from a large sample of radio galaxies with redshifts $0.1 < z < 3$; he showed that the emission-line spectra of these more distant (more radio-powerful) sources are also consistent with being photoionized, but as Villar-Martín, Tadhunter & Clark (1997) argued, this composite spectrum is dominated by the few most highly ionized galaxies and so this result does not necessarily apply to the population as a whole. This photoionization mechanism is in complete agreement with the currently popular orientation-based unification schemes of radio galaxies and radio-loud quasars (e.g. Barthel 1989) in which all radio galaxies should host a powerful obscured AGN, supplying a large flux of anisotropically emitted ionizing photons. The presence of such an obscured quasar nucleus is also indicated by the detection of spatially extended polarized emission and broad permitted lines in polarized light, as a result of scattering of the AGN light by electrons or dust (see Antonucci 1993 for a review).

Photoionization is not the only story, however. As reviewed by Binette, Wilson & Storchi-Bergmann (1996), simple photoionization models fail to reproduce some important features of the emission-line spectra of the narrow-line regions of active galaxies. In particular, the strengths of many high-excitation lines (e.g. [Ne V] 3426, C IV 1549, and high-ionization Fe lines) are underpredicted by factors as large as 10, the electronic temperatures derived by simple photoionization models are too low when compared with those inferred from the line ratio [O III] 4363 / [O III] 5007, and photoionization models alone cannot reproduce the large observed scatter in the He II 4686 / Hβ ratio. Moreover, a significant fraction of radio galaxies show indications of interactions between the radio jets and the surrounding emission-line gas, with the radio source shocks determining the morphology and kinematics of the gas. Detailed studies of individual sources (e.g. PKS 2250 − 41, $z = 0.31$: Clark et al. 1997; Villar-Martín et al. 1999; 3C 171, $z = 0.24$: Clark et al. 1998) have shown that in some regions of the source, the shocks can also dominate the ionization; for example, minima in the ionization state are observed coincident with the radio hotspots, and an anticorrelation is found between the ionization state of the extended gas and its (jet-shock broadened) line width.

At high redshifts, $z \gtrsim 0.6$, interactions between the radio jets and the gas are readily apparent from the kinematics of the ionized gas (see Section 3, below). What has not been clear, however, is the extent to which the shocks play a role in the ionization of these high-redshift sources.

2.1 The C III] 1909 / C II] 2326 versus [Ne III] 3869 / [Ne V] 3426 diagram

Line ratio diagnostic diagrams, pioneered by Baldwin, Phillips & Terlevich (1981), provide a powerful tool for investigating the ionization mechanism of emission-line gas. They have been widely used to distinguish the extended emission-line regions of active nuclei from H II regions and planetary nebulae, and in recent years also between shock and photoionization models for AGN. Standard emission-line diagnostics at rest frame optical wavelengths are shifted in to the near-infrared wavebands for redshifts $z \gtrsim 1$, and so cannot easily be used for high-redshift radio galaxies. In the past couple of years, however, new diagnostic diagrams have been constructed for rest frame UV emission-lines redshifted into the optical window (Villar-Martín et al. 1997; Allen, Dopita & Tsvetanov 1998).

The emission-line pairs C III] 1990 & C II] 2326 and [Ne III] 3869 & [Ne V] 3426 are well-suited for use as line ratio diagnostics for distant radio galaxies for a number of reasons. All four of these fairly high excitation lines are relatively strong in AGN spectra, and so their fluxes can be determined with sufficient accuracy even for high-redshift radio galaxies. The two lines in each pair involve the same element, and therefore there is no dependence of the line ratios on metallicity or abundances; they are also close in wavelength, and so the effects of differential reddening or calibration errors are minimized. Perhaps most importantly, the predictions of shock and photoionization models for these line ratios are significantly different.

The line ratio C III]1909 / C II] 2326 was determined for 13 of the 14 sources in the sample from the data presented in Paper I; the values of this ratio are given in Table 1 together with many

Table 1. Ionization and kinematic properties of the radio galaxies, as calculated from the data presented in Paper I. Column 1 gives the radio source name and column 2 its redshift. The projected linear size of the radio source (from Best et al. 1997) is given in column 3. The emission-line ratios of C III] 1909 / C II] 2326 and [Ne III] 3869 / [Ne V] 3426, together with their uncertainties, are given in columns 4 to 7. The integrated [O II] 3727 flux density is given in column 8 and its equivalent width in the rest frame of the source is in column 9. The projected linear extent of the emission-line region along the direction of the slit is in column 10. Column 11 gives the maximum FWHM of the [O II] 3727 emission-line in the spectrum, column 12 the range in relative velocities of this line seen along the slit, and column 13 the number of distinct velocity components, as described in the text. Column 14 gives the extent of the aligned optical emission from the *HST* images of Best et al. (1997).

Source	z	Radio size [kpc]	C III]/C II] ratio	error	[Ne III] / [Ne V][a] ratio	error	[O II] flux ($\times 10^{-15}$) [erg/s/cm^2]	Eq. width [Å]	Emis. size [kpc]	Max. FWHM [km/s]	Vel. range [km/s]	No. comps [kpc]	Opt. size [kpc]
(1)	(2)	(3)	(4)	(5)	(6)	(7)	(8)	(9)	(10)	(11)	(12)	(13)	(14)
3C 22	0.935	208	4.8	0.9	1.4	0.4	2.02	80	41	875	75	1	16
3C 217	0.898	110	1.3	0.2	5.0	2.2	4.85	544	57	1000	175	3	21
3C 226	0.818	263	1.9	0.3	–	–	1.21	159	50	725	425	1	19
3C 247	0.749	113	2.3	0.9	–	–	1.24	129	77	850	250	3	43
3C 252	1.104	488	2.6	0.4	–	–	0.81	125	56	450	250	1	22
3C 265	0.810	646	6.4	0.9	1.2	0.5	3.56	191	111	700	725	4	76
3C 280	0.997	117	4.8	0.8	0.7	0.3	2.11	173	102	800	650	4 ± 1	22
3C 289	0.967	89	2.8	0.5	–	–	0.78	149	46	675	75	1	16
3C 324	1.208	96	2.4	0.7	6.2	1.0	1.93	219	60	1025	800	2[b]	25
3C 340	0.775	371	10.1	1.9	0.8	0.3	0.58	84	47	600	200	1	24
3C 352	0.806	102	1.7	0.3	4.0	1.5	2.57	295	78	1050	800	3	24
3C 356[c]	1.079	624	8.4	1.5	0.9	0.2	0.76	111	32	725	50	1	12
3C 368	1.132	73	1.1	0.2	3.9	0.5	5.87	202[d]	86	1350	600	3 ± 1	58
3C 441	0.708	211	–	–	1.0	0.3	0.47	58	33	900	375	1	18

Notes:
[a] Values of the [Ne III] 3869 / [Ne V] 3426 ratio are taken from: 3C 22 – Rawlings et al. (1995); 3C 217 & 3C 340 – Spinrad, private communication; 3C 265 & 3C 352 – Smith et al. (1979); 3C 280 – Spinrad (1982); 3C 324 – Paper I; 3C 356 – Lacy & Rawlings (1994); 3C 368 – Stockton, Ridgway & Kellogg (1996); 3C 441 – Lacy et al. (1998).
[b] For 3C 324 this corresponds to the two kinematically distinct components at $+400$ and $-400\,\mathrm{km\,s^{-1}}$.
[c] The data for 3C 356 are for a more northerly galaxy.
[d] For 3C 368 the determined equivalent width is a lower limit because of the contribution of the M star (Hammer, Le Fèvre & Proust 1991) to the continuum level.

other derived quantities of the radio galaxies. For the lowest redshift source, 3C 340, C III] 1909 is not redshifted to a sufficiently high wavelength to be observed. The ratio [Ne III] 3869 / [Ne V] 3426 is only available from the Paper I data for the source 3C 324, but for nine of the other sources in the sample, values are available from the literature; these also are compiled in Table 1. The two line ratios are plotted against each other on Fig. 1, where they are compared to the theoretical predictions of shock and photoionization as discussed in the following subsections.

2.2 Photoionization models

The theoretical line ratios of C III] 1909 / C II] 2326 and [Ne III] 3869 / [Ne V] 3426 for photoionized gas were taken from the work of Allen et al. (1998), who calculated the predicted line ratios for a number of emission-lines using the MAPPINGS II code (Sutherland, Bicknell & Dopita 1993). Allen et al. considered a planar slab of gas illuminated by a power-law spectrum of ionizing radiation, and calculated the emission-line ratios for a wide range of conditions: for two different spectral indices of the input spectrum ($F_\nu \propto \nu^\alpha$ with $\alpha = -1$ and $\alpha = -1.4$), and two different densities of cloud ($n_\mathrm{e} = 100$ and $1000\,\mathrm{cm^{-3}}$), the ionization parameter U[1] was allowed to vary in the range $10^{-4} \leq U \leq 1$. A high energy cut-off was applied to the ionizing spectrum at 1.36 keV to avoid overproducing the intensity of the soft X-rays. The models are ionization bounded and correspond to a range in cloud sizes from 0.003 to 32 parsec. The resultant line ratio sequences are shown on Fig. 1.

It is beyond the scope of this paper to provide a more detailed description of the photoionization models, or of the other theoretical models considered next. For more complete discussions of these modelling techniques the reader is referred to the papers from which the theoretical line ratios have been drawn, in this case the work of Allen et al. (1998).

2.3 Photoionization including matter bounded clouds

To avoid the shortcomings of simple photoionization models discussed at the beginning of Section 2, Binette et al. (1996) considered photoionization of a composite population containing both optically thin (matter bounded; MB) and optically thick (ionization bounded; IB) clouds (cf. Viegas & Prieto 1992). In their models, all of the photoionizing radiation passes initially through the MB clouds which absorb a fraction ($F_\mathrm{MB} \sim 40$ per cent) of the impinging ionizing photons and produce the majority of the high-ionization lines in the spectrum. The radiation which is not absorbed then strikes the population of IB clouds; this radiation has already been filtered by the MB clouds as a result of which the IB clouds give rise to predominantly low and intermediate excitation lines. According to these models, the variation in the emission-line ratios from galaxy to galaxy has its origin in the variation of the ratio (hereafter $A_\mathrm{M/I}$) of the solid angle from the photoionizing source subtended by MB clouds

[1] The ionization parameter U is defined as the ratio of the number density of ionizing photons striking the cloud to the gas density (n_H) at the front face of the cloud [$U = (cn_\mathrm{H})^{-1}\int_{\nu_0}^{\infty}(F_\nu \mathrm{d}\nu)/h\nu$], where c is the speed of light and ν_0 is the ionization potential of hydrogen.

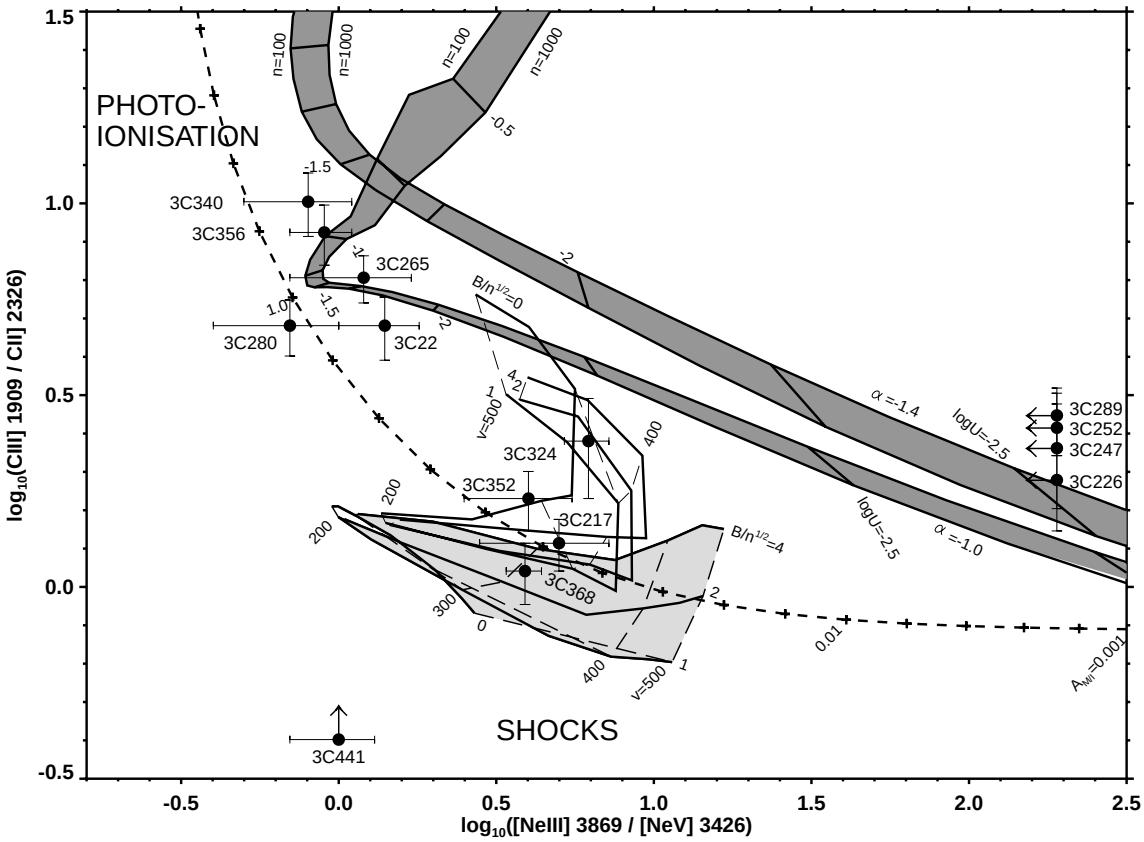

Figure 1. An emission-line diagnostic plot for the 3CR radio galaxies, compared with theoretical predictions. The upper shaded regions correspond to simple photoionization models ($\alpha = -1.0$ and $\alpha = -1.4$), as described in Section 2.2. The dashed line corresponds to the sequence for photoionization models including matter-bounded clouds described in Section 2.3. The lower shaded region covers the ratios predicted by the shock models described in Section 2.4; the unshaded region just above this corresponds to the shock models including a precursor region (see Section 2.4). The five galaxies plotted towards the edge of the diagram have no data available for one of their emission-line ratios. An interpretation of this diagram can be found in Section 2.5.

relative to that of IB clouds. A larger value of $A_{\rm M/I}$ corresponds to a larger weight given to the MB clouds and hence a higher excitation spectrum. Since the model states that all of the ionizing radiation striking the IB clouds must first have passed through the MB clouds, the ratio $A_{\rm M/I}$ strictly cannot be below unity.

Binette et al. (1996) consider two physical situations which might produce such a composite cloud population (some combination of the two would also be possible): (i) the MB 'clouds' may be optically thin shells surrounding a denser IB core of a cloud; (ii) the MB clouds could be a separate population of clouds which lie close to the ionizing source. In the second case, the MB clouds would have to have a covering factor of unity in order that all lines of sight to the IB clouds pass through a MB cloud; this is possible for very small clouds, consistent with the fact that they would be optically thin. Note that in the case of the MB clouds forming a separate cloud population, if some fraction of them are obscured from the observer, for example by the same material that obscures the active nucleus itself, this may give rise to an apparent $A_{\rm M/I} < 1$.

Binette et al. (1996) tabulated the line ratios in the two cloud populations for a single set of parameters, chosen to give a good match to Seyfert spectra. They adopted a power-law spectrum with a spectral index of $\alpha = -1.3$ ($F_\nu \propto \nu^\alpha$), ionization parameters of $U_{\rm MB} = 0.04$ and $U_{\rm IB} = 5.2 \times 10^{-4}$, a density in the MB clouds of $50\,{\rm cm}^{-3}$, and absorbed ionizing photon fractions of $F_{\rm MB} = 0.4$ and $F_{\rm IB} = 0.97$ (see their paper for a more detailed discussion of these quantities). From these data, a sequence of line ratios of C III] 1909 / C II] 2326 and [Ne III] 3869 / [Ne V] 3426 have been calculated allowing the quantity $A_{\rm M/I}$ to vary in the range $0.001 \leq A_{\rm M/I} \leq 100$; this sequence is shown in Fig. 1.

2.4 Shock ionization models

Fast radiative shocks are a powerful source of ionizing photons which can have a profound influence upon the temperature and ionization properties of the gas in the post-shock region. An overview of shock ionization models is provided by Dopita & Sutherland (1996). The two most important parameters for controlling the post-shock emission-line spectrum are the velocity of the shock and the ratio $B/\sqrt{n}$, where B is the pre-shock transverse magnetic field and n is the pre-shock number density of the emission-line clouds. The latter ratio controls the density, and hence the effective ionization parameter, of the post-shock gas, since at high shock velocities the transverse magnetic field limits the compression caused by the shock through a balance between the magnetic pressure of the cloud ($\propto B^2$) and the ram pressure of the shock ($\propto n$).

Dopita & Sutherland (1996) calculated the emission-line ratios expected from gas ionized by the photons produced in shocks for a range of physical conditions: the velocity of the shock through the emission-line clouds was allowed to vary from 150 to 500 km s^{-1},

and the 'magnetic parameter' was varied in the range $0 \leq B/\sqrt{n} \leq 4\,\mu\mathrm{G\,cm^{-1.5}}$, which spans the expected range of values (see their paper for more details). These authors also emphasized the importance of photons produced by the shock diffusing upstream and ionizing the pre-shock gas. This may give rise to extensive precursor emission-line regions, with different spectral characteristics to the compressed shocked gas. They therefore calculated the emission-line spectra predicted for these precursor regions for a range of shock velocities from 200 to 500 km s^{-1}. In distant radio galaxies such as the ones studied in this paper, the spatial resolution is insufficient to distinguish between the precursor and post-shock emission regions, and a combined spectrum of the two would be observed.

Using the data tables provided by Dopita & Sutherland, the emission-line ratios of C III] 1909 / C II] 2326 and [Ne III] 3869 / [Ne V] 3426 were calculated both for simple shock models and for shock models including a precursor region. These theoretical ratios are shown on Fig. 1.

2.5 Interpreting the line diagnostic diagram

Fig. 1 clearly demonstrates that the ionization states of radio galaxies, even within a tightly defined sample such as the one studied here, show considerable variations: the C III] 1909 / C II] 2326 ratio differs by nearly a factor of 10 between 3C 368 and 3C 340. The nine sources for which ratios are available for both lines clump into two groups of sources; 3C 217, 3C 324, 3C 352 and 3C 368 are grouped together in the region corresponding to the shock ionization models, while 3C 22, 3C 265, 3C 280, 3C 340 and 3C 356 are all close to the photoionization predictions. Interestingly, the four sources in the first region all have projected radio linear sizes smaller than 115 kpc and the five sources in the second group all have sizes larger than this value. This result is more apparent in Fig. 2 where the ratio of C III] 1909 / C II] 2326[2] is plotted against the linear size of the radio source; the two parameters are correlated at the 98.5 per cent significance level in a Spearmann–Rank test.

For all nine sources, the photoionization models of Binette et al. (1996) including matter-bounded clouds provide an acceptable fit to the data. There is, however, a problem with this model. As discussed in Section 2.3, a value of $A_{\mathrm{M/I}} < 1$ is only possible if the MB clouds form a separate population of clouds, some of which are obscured from the observer. The four small radio sources would have to have a value $A_{\mathrm{M/I}} \approx 0.1$, implying that over 90 per cent of their MB clouds are obscured, while there is no requirement for obscuration of the larger radio sources ($A_{\mathrm{M/I}} \approx 1$). The amount of obscuration would therefore have to depend upon the size of the radio source.

Three factors determine the projected linear size of a radio source: the orientation of the source with respect to the line of sight, the age of the radio source and the advance rate of the hotspots. The first of these cannot be responsible since sources orientated more towards the line of sight, hence appearing smaller, will have less, not more, obscuration towards their central regions (cf. orientation-based schemes of radio galaxies and radio-loud quasars). Although the second option cannot be excluded, it seems improbable that the obscuration of MB clouds in the central regions will decrease by an order of magnitude during the short time-scale of a radio source lifetime (a few $\times 10^7$ yr) without the same process either destroying the clouds themselves or having other consequences, for example for the visibility of the broad-line regions. The third possibility, that there may be a connection between a higher obscuration of the central regions of small radio sources and a slower advance rate of their hotspots, has parallels with the suggestion that compact symmetric radio sources are small because they are confined by a dense (obscuring) surrounding medium (e.g. van Breugel, Miley & Heckman 1984). However, recent investigations of compact radio sources using very long baseline interferometry (VLBI) techniques have derived hotspot advance velocities of significant fractions of the speed of light ($\approx 0.2c$, e.g. Owsianik & Conway 1998; Owsianik, Conway & Polatidis 1998), supporting a youth rather than confinement scenario for these sources. This indicates that there is no strong connection between hotspot advance speed and obscuration (density) of the central regions of radio sources.

It seems unlikely, therefore, that the value of $A_{\mathrm{M/I}}$ should be strongly dependent upon the radio source size. Although this possibility cannot categorically be excluded, our preferred interpretation of the line diagnostic diagram is that for four sources, for which the extent of the emission-line region is within a factor of two of the radio source size, the ionization is dominated by shocks, whilst for the other five sources photoionization dominates. This interpretation will be supported by the discussion of the kinematics in the following section; the matter-bounded cloud photoionization model would provide no clear explanation of the variations seen in the kinematical properties.

The uncertainties in the emission-line ratios for each individual galaxy are too large to pin down any parameters of the ionization accurately, but one feature is readily apparent. The five sources in the photoionization region of the diagram are significantly more consistent with a flatter spectral index ($\alpha \approx -1.0$) for the power-law ionizing continuum than with the steeper one ($\alpha \approx -1.4$) typically adopted for low-redshift sources. Villar-Martín et al. (1997) found a similar result analysing the rest frame UV emission-lines of radio galaxies with redshifts $z > 1.7$, suggesting that this may be a general feature of high redshift AGN.

3 MORPHOLOGICAL AND KINEMATICAL PROPERTIES OF THE EMISSION-LINE GAS

The emission-line gas surrounding low redshift radio galaxies shows velocity shears within the galaxies of between 50 and 500 km s^{-1}, and (deconvolved) full width at half maximum (FWHM) values of the emission-lines typically in the range 200 to 600 km s^{-1} (Tadhunter, Fosbury & Quinn 1989b; Baum et al. 1992). In many cases the kinematics are consistent with a gravitational origin. At high redshifts the kinematics can be much more extreme, with velocity dispersions often in excess of 1000 km s^{-1} (McCarthy et al. 1996; Paper I) and components offset by several hundreds of km s^{-1} with respect to bulk of the gas (Tadhunter 1991; Paper I). These remarkable kinematics are inconsistent with gravitational origins (cf. Tadhunter 1991). In this section the variation in the kinematics is compared with other properties of the radio source to investigate their origin.

In Table 1 a number of the parameters of the emission-line

[2] This ratio is preferred to the [Ne III] 3869 / [Ne V] 3426 ratio here, and in later figures, because data are available for more of the galaxies and because the ratios are all drawn from the homogeneous data set presented in Paper I. The Neon ratio provides similar results, as is apparent from the strong inverse correlation between the two ratios seen on Fig. 1.

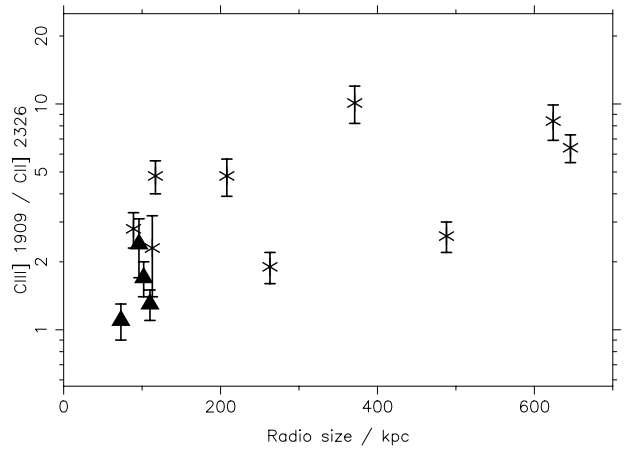

Figure 2. The correlation between the C III] 1909 / C II] 2326 emission-line ratio and the projected linear size of the radio source. The four sources lying in the 'shocks' region of the line diagnostic diagram, Fig. 1, are plotted as filled triangles and the remainder of the galaxies as asterisks.

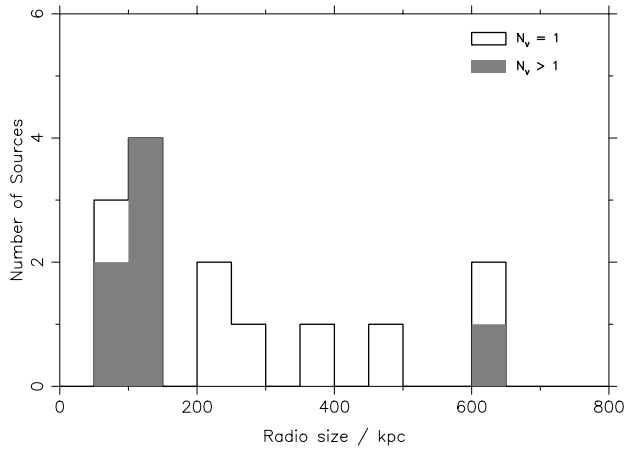

Figure 3. A histogram of the radio size distribution of the sources, separated into sources with smooth velocity profiles ($N_v = 1$, unshaded) and those with irregular profiles ($N_v > 1$, shaded).

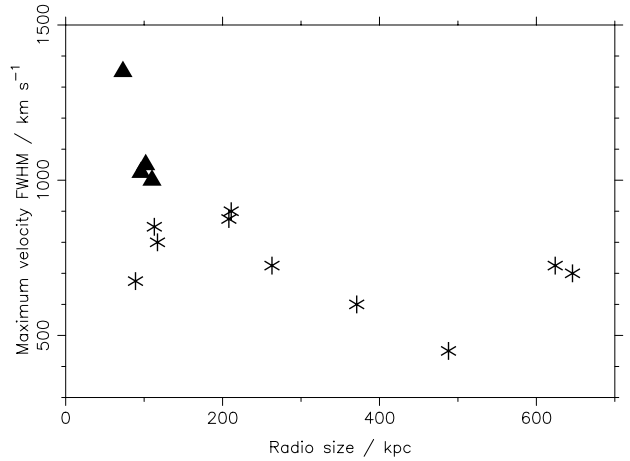

Figure 4. The inverse correlation between the maximum FWHM of the [O II] 3727 emission-line and the projected linear size of the radio source. Symbols as in Fig. 2.

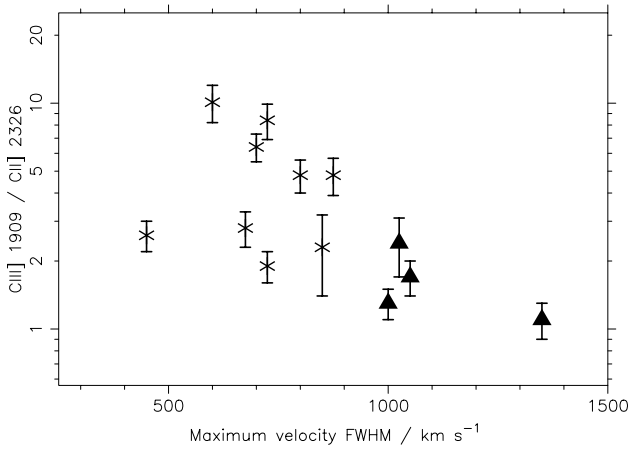

Figure 5. A plot showing the direct connection between the ionization state of the emission-line gas, as indicated by the C III] 1909 / C II] 2326 line ratio, and its kinematics in terms of the emission-line maximum FWHM. Symbols as in Fig. 2.

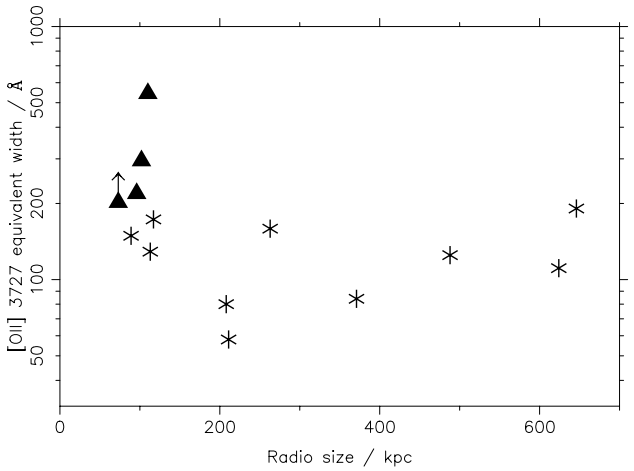

Figure 6. The decrease in the equivalent width of the [O II] 3727 emission-line with increasing size of the radio source. Symbols as in Fig. 2. 3C 368 is plotted as a lower limit because of the contribution of the M star to its continuum level.

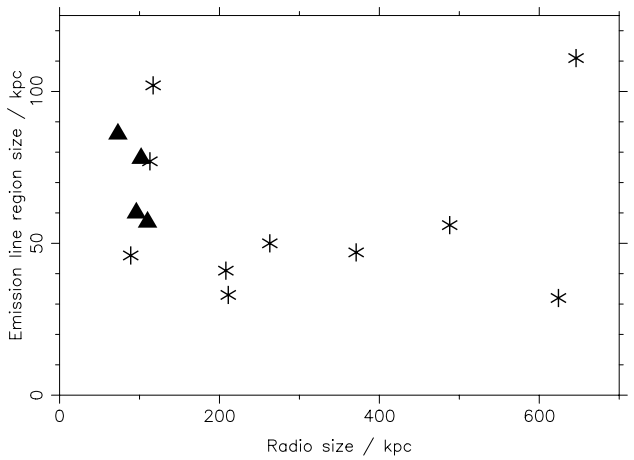

Figure 7. The variation of the linear extent of the [O II] 3727 emission-line region with the size of the radio source. Symbols as in Fig. 2.

properties of the gas are provided. The integrated [O II] 3727 emission-line intensity and the rest frame equivalent width of this emission-line are as calculated in Paper I. The projected linear size of the emission-line region along the slit direction was determined from the extent of the locations at which fits to the [O II] 3727 emission-line profile were obtained in figs 2 to 15(d) of Paper I (excluding the detached emission-line systems for 3C 356 and 3C 441). The range in relative velocities was calculated, to the nearest 25 km s^{-1}, from figs 2 to 15(e) of Paper I, considering the velocity separation between the most positive and most negative velocity components of the [O II] 3727 emission-line, excluding any data points with uncertainties greater than 100 km s^{-1}. The maximum value of the FWHM of the emission-line gas was determined from figs 2 to 15(f) in Paper I, again excluding any locations with uncertainties greater than 100 km s^{-1}.

One further parameter was calculated, hereafter referred to as the 'number of velocity components', N_v, to provide an indication of the smoothness of the velocity profile. N_v was defined as the number of single velocity gradient components (i.e. straight lines) necessary to fit, within the errors, the velocity profiles along the slit direction (Figs 2 to 15e of Paper I; cf. van Ojik et al. 1997). A galaxy the mean motion of which is consistent with simple rotation will provide a single component fit; higher values of N_v correspond to irregular motions. This analysis, being by its very nature somewhat subjective, was carried out separately by two of the authors and by a third independent scientist. For 11 of the 14 galaxies, a unanimous value of N_v was obtained. The remaining three galaxies show more complicated profiles and their classification is ambiguous: for 3C 280, values of 3, 4 and 5 were obtained, and so a value of 4 ± 1 is adopted; for 3C 324 the profile is very different from the other galaxies, being composed of two kinematically distinct systems as discussed in Paper I – a value of 2 is used; values of 2, 3 and 4 were assigned to 3C 368, and so 3 ± 1 is adopted. The precise values of N_v for these galaxies are of less importance than the fact they they are clearly inconsistent with a value of 1. The values of N_v are compiled in Table 1.

A number of features are immediately apparent from Table 1. It is noteworthy that of the seven galaxies with projected radio sizes smaller than 150 kpc, six have values $N_v > 1$ with only one having $N_v = 1$, while six of the seven sources larger than this size have $N_v = 1$ (see Fig. 3). A χ^2 test shows that the probability of this occurring by chance is below 1 per cent. Small radio sources predominantly have emission-line gas with distorted velocity profiles, and the emission-line gas of large radio sources has a velocity profile generally consistent with rotation.

A similar result is found with the variation of the maximum FWHM with radio size, shown in Fig. 4. These two parameters are anti-correlated at greater than the 99 per cent significance level (Spearmann Rank test), with the four sources lying in the 'shock' region of the line diagnostic diagram (Fig. 1) having clearly the highest values. This latter point is made more clearly in Fig. 5 where the FWHM of the [O II] 3727 emission can be seen to be inversely correlated with the C III] 1909 / C II] 2326 emission-line ratio, at the 98.5 per cent significance level using a Spearmann Rank correlation test. The kinematical and ionization properties of these galaxies are fundamentally connected.

It is not only the kinematics of the gas that evolve with the radio source size, but also the physical extent and the luminosity of the line emission. Fig. 6 shows the variation of the equivalent width of the [O II] 3727 emission-line with increasing size of the radio source. Although this correlation is less strong (96 per cent significance in a Spearmann Rank test), it is apparent that the small sources in the 'shock-dominated' region of Fig. 1 show enhanced [O II] 3727 equivalent widths. A more accurate description of Fig. 6 is not that there is an inverse correlation between the equivalent width of the [O II] emission and radio size, but rather that at large ($\gtrsim$150 kpc) radio sizes the distribution of equivalent widths is fairly flat, and at small sizes there is often a factor of 2 to 3 excess emission relative to this level.

This enhancement of the line *equivalent widths* of small radio sources with respect to large sources implies an even greater boosting of their line *luminosities*, for two reasons. First, the optical continuum emission of small radio sources is more luminous than that of large sources, as indicated by Best et al. (1996), decreasing the apparent increase in the emission-line equivalent width. Secondly, the equivalent width is determined from the extracted one-dimensional spectrum from a spatial region along the slit of about 35 kpc (see Paper I); the physical extent of the emission-line regions of small radio sources is greater than that of large radio sources, as shown in Fig. 7. Excluding 3C 265, which is an exceptional source in many ways (e.g. see discussion in Best et al. 1997), the emission-line regions of radio sources with sizes $\gtrsim$200 kpc have total extents of up to about 50 kpc (25 kpc radius, if symmetrical). Smaller radio sources, however, have emission-line regions ranging from this size up to about 100 kpc, a size comparable to the extent of the radio source. In other words, line emission at distances from the AGN of 30 to 50 kpc generally is only seen at the stage of radio source evolution when the hotspots are passing, or have just passed, through this region.

4 DISCUSSION

A number of results have been derived in the previous sections and these are summarized here for clarity.

(i) Radio sources with small linear sizes ($\lesssim$120 kpc) have lower ionization states than larger radio sources. Their emission-line ratios are in agreement with the theoretical predictions of shock ionization models, whilst those of large radio sources are consistent with photoionization.

(ii) There is a strong inverse correlation between the FWHM of the [O II] 3727 emission and the size of the radio source. The four sources with 'shock-dominated' ionization states have the highest FWHM.

(iii) Large radio sources often have smooth velocity profiles consistent with rotation, whilst those of small sources are more distorted.

(iv) The [O II] 3727 emission-line strength correlates inversely with the radio source size. The four 'shock-dominated' sources have the highest integrated [O II] 3727 equivalent widths.

(v) The physical extent of the line-emitting regions is larger in smaller radio sources.

Before discussing the interpretation of these correlations, first a comparison is made to see if such results also hold for low-redshift radio galaxies.

4.1 Comparison with low-redshift radio galaxies

Baum et al. (1992) studied the ionization and kinematics of a sample of 40 radio galaxies with redshifts $z \lesssim 0.2$. Their sample contained a large mixture of radio source types, including both

Table 2. Selected properties of the low redshift sample of FR II radio sources studied by Baum et al. (1992).

Source	Radio size [kpc]	Kinematic class[a]	[O I] 6300.3 / Hα ratio	error
3C 33	397	R	0.20	0.08
3C 63	84	VNR	0.28	–[b]
3C 98	264	R	0.12	0.01
PKS 0634–206	1200	R	0.06	0.01
3C 192	308	R	0.10	–[b]
3C 227	499	R	–	–
3C 285	268	R	0.15	0.09
3C 403	357	R	0.21	0.16
3C 405	194	CNR	0.32	0.08
3C 433	169	VNR	0.23	0.03
PKS 0349–278	635	R	–	–
3C 171	171	VNR	–	–
3C 184.1	473	R	–	–
3C 277.3	106	VNR	–	–
4C 29.30	85	VNR	–	–
3C 293	261	R	–	–
3C 305	15	R	–	–
3C 382	287	R	–	–

Notes:
[a] R – rotator; CNR – calm non-rotator; VNR – violent non-rotator.
[b] No error quoted as the mean value is taken from data at only one position.

Fanaroff & Riley (1974; hereafter FR) class I and II objects[3] as well as sources with intermediate structures. Many differences are now known to exist between the FR I and FR II sources besides the large differences at radio wavelengths, such as the luminosity and environments of their host galaxies (Hill & Lilly 1991; Baum, Zirbel & O'Dea 1995; Ledlow & Owen 1996), the luminosity of their emission-line gas (Zirbel & Baum 1995), differences in the dust properties (de Koff et al. 2000), and possibly a different mode of accretion on to the central black hole (Reynolds et al. 1996).

Baum et al. also found a significant difference in the host galaxy kinematics between the two radio source types. They classified the kinematics of the radio galaxies into three classes, 'rotators', 'calm non-rotators' and 'violent non-rotators'. They found that almost all of the FR II sources fell into the rotator or violent non-rotator classes; most of the FR I and intermediate type sources were calm non-rotators. All of the FR IIs had strong emission-lines with a relatively high ionization parameter, whilst the FR I and intermediate class sources had much weaker emission-lines of lower ionization, with the surrounding hot interstellar and intracluster medium likely to play an important role in the ionization, both through heat conduction and through ionization by its ultraviolet and soft X-ray emission (see also Baum et al. 1995; Zirbel & Baum 1995). Given the large differences between FR I and FR II sources, to allow a direct comparison with the high redshift sample, attention here is restricted to only the FR II sources in their sample. Four FR IIs in the sample lie more southerly than declination $-30°$, and for two of these, accurate determinations of the radio size could not be found in the literature; to avoid introducing any biases by selecting only the well-studied sources, all four of these sources have been excluded from further consideration.

The remaining sample of low redshift FR II radio galaxies is listed in Table 2, along with the linear size of the radio source taken from the literature and the kinematic classification given by Baum et al. (1992). In Fig. 8 a histogram of the linear sizes is presented, separating the rotator and non-rotator classes. It is clear that the non-rotator classes are associated with small radio sources, and the rotator class with larger sources, exactly as is found for the high-redshift sample. The only exception to this rule is 3C 305, which is a rotator with a small radio size: indeed, this is the smallest radio source in the sample (15 kpc), and it could be argued that any shocks associated with the radio source have not yet passed through a significant proportion of the host galaxy, accounting for the lack of clear non-rotational kinematics. Even including 3C 305, the probability of the radio sizes of the rotator and non-rotator classes being drawn from the same parent samples is less than 0.5 per cent (using a Mann–Whitney U-test).

All of the FR IIs in the sample have relatively high ionization states, but differences are seen from galaxy to galaxy. Baum, Heckman & van Breugel (1990) present the line strengths of the [O I] 6300.3, [N II] 6548.1,6583.4, Hα and [S II] 6716.4,6730.8 emission-lines as a function of position for half of the sample considered in their 1992 paper. Although these are all relatively low ionization lines and therefore not the most sensitive to

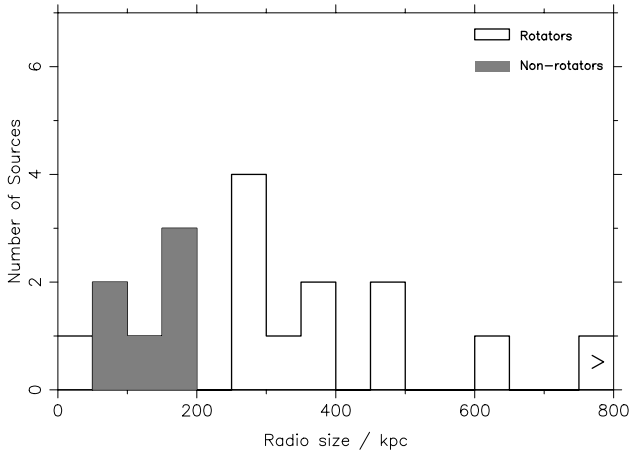

Figure 8. A histogram of radio sizes for the different kinematic classifications of the FR II radio galaxies in the low-redshift Baum et al. (1992) sample.

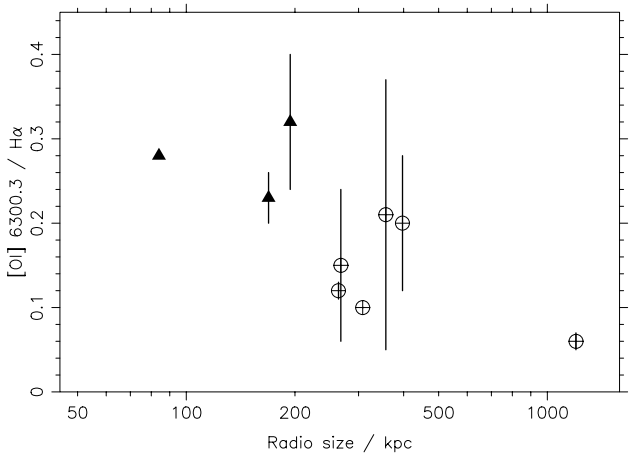

Figure 9. A plot showing the anticorrelation between the radio size and the ionization state for the FR IIs in the low redshift Baum et al. (1992) sample. The rotators are represented by the crossed circles and the non-rotators by the filled triangles.

[3] FR I radio sources are edge-darkened sources of generally lower radio luminosity than the FR II sources; FR IIs are characterized by bright hotspots towards the extremities of each lobe.

differences between shock and photoionization, the [O I]/Hα ratio should be somewhat higher for shock ionized gas than for photoionized gas. An 'average' value of this emission-line ratio has been calculated for each galaxy as the mean of the ratios at the various positions tabulated by Baum et al. (1990); these are given in Table 2, the errors quoted representing the scatter in the ratio with location in the galaxy. In Fig. 9 these ratios are plotted against radio size: a Spearmann Rank test shows that this emission-line ratio is anticorrelated with radio size at the 96 per cent confidence level.

The low-redshift sample therefore provides results similar to those of the high-redshift sample. Large FR II radio sources have kinematics consistent with rotation and higher ionization states than small radio sources, the ionization and kinematics of which show more evidence for the role of shocks. It is of note that the low and intermediate redshift sources for which individual studies have shown unambiguously that the kinematics and ionization are dominated by shocks are almost invariably cases in which the radio source is of comparable size to the extended emission-line regions (e.g. Clark et al. 1997, 1998), naturally agreeing with this picture.

One significant difference that remains between the low- and high-redshift samples is that the high-redshift sources are more extreme in their emission-line properties (luminosities, line widths, etc.) than are those at low redshifts. The most important factor influencing this is the sharp increase of the radio power with redshift in the flux-limited samples, with corresponding increases in both the flux of ionizing photons from the AGN and the energy of the jet shocks. However, Tadhunter et al. (1998) investigated the correlations of different emission-line strengths with redshift and showed that this cannot be the only reason: the ionization-sensitive [O II] 3727/[O III] 5007 ratio does not decrease strongly with redshift as it should if the only difference between the low-power, low-redshift and the high-power, high-redshift objects was that the latter contained a more luminous photoionizing source. They concluded that a secondary effect, such as an increase in the density of the intergalactic medium or an increase in the importance of jet-cloud interactions with redshift, is also required.

4.2 The role of shocks in small sources

The results presented in the previous sections, coupled with the evidence that a similar situation is seen at low redshifts, lead naturally to a single scenario to explain all of the emission-line properties.

For small radio sources, the morphology, kinematics and ionization properties of the emission-line gas are dominated by the effects of the bow shock associated with the expansion of the radio source. As this bow shock passes through the interstellar and intergalactic medium (ISM and IGM), the intercloud gas is quickly accelerated to the velocity of the bow shock, but the warm emission-line clouds are essentially bypassed by the shock front (e.g. Rees 1989; Begelman & Cioffi 1989). The clouds are accelerated during the short time it takes the shock to pass the cloud by, as a result of the imbalance in the pressures between the pre-shock and post-shock gas on the front and back of the cloud. The velocity to which the clouds are accelerated in this way is easily shown to be independent of cloud size and to be well below 100 kms (e.g. Rees 1989).

Much larger velocities are induced, however, if the effect of ram-pressure acceleration by the shocked IGM gas (often referred to as entrainment) is considered. Behind the initial bow shock, the clouds find themselves in a shocked layer of IGM, moving outwards at speeds approaching that of the bow shock. The clouds will be accelerated within this medium until they pass across the contact discontinuity into the radio cocoon, where the pressure is the same as in the shocked layer of gas but the density is much lower, and they are no longer accelerated; there is essentially no mixing of the hot intercloud gas across this contact discontinuity (e.g. Norman et al. 1982).

During the time ΔT for which a cloud is between the bow shock and the contact discontinuity, the momentum imparted to the cloud by the shocked IGM can be approximated to first order as $r_c^2 v_s^2 n_g m_p \Delta T$, where r_c is the cloud size, v_s is the bow shock velocity, n_g is the post-shock number density of the intercloud gas and m_p is the proton mass. The mass of the cloud is of order $r_c^3 n_c m_p$, where n_c is the cloud number density, and the time-scale ΔT is of order D/v_s, where D is the distance between the bow-shock and the contact discontinuity; therefore, the velocity to which the cloud is accelerated is

$$v_c \sim \frac{D}{r_c}\frac{n_g}{n_c} v_s. \quad (1)$$

In the radio source evolution models of Kaiser & Alexander (1997), radio sources grow self-similarly and D is found to be about 3 per cent of the distance between the AGN and the bow shock (Kaiser & Alexander 1999); for the radio source passing through the emission-line region at radius $\sim$15 kpc then, $D \sim 0.5$ kpc. Assuming a density ratio of $n_g/n_c \sim 10^{-4}$ for pressure equilibrium between the clouds ($T \sim 10^4$ K) and the surrounding IGM ($T \sim 10^8$ K), and a shock velocity of $v_s \sim 0.05c$ from typical hotspot advance velocities (e.g. Liu, Pooley & Riley 1992), then a cloud of size $r_c \sim 1$ pc will be accelerated to 750 km s^{-1}, comparable to the velocities observed in the small radio sources (the actual velocities may need to be slightly higher since the radio galaxies are believed to lie close to the plane of the sky). The spread in projected cloud velocities from clouds of different sizes and from clouds accelerated through different regions of the bow shock will lead to the broad velocity dispersions. The acceleration of the emission-line gas clouds by the radio bow shocks therefore explains the distorted velocity profiles and large line widths observed in small radio sources.

It is interesting to note that the acquired cloud velocities are proportional to the bow-shock velocity v_s. If the bow-shock velocity increases with radio power (redshift), as has been suggested from spectral ageing measurements of hotspot advance velocities (e.g. Liu et al. 1992), this would explain why greater velocity widths are seen in high-redshift sources than in low-redshift sources.

The ionization state of the large radio sources indicates that the dominant source of ionizing photons in these sources is the AGN. Since the properties of the AGN are not expected to change dramatically between small and large radio sources, the gas surrounding the small sources should receive a similar flux of photoionizing radiation. The lower ionization state seen in the spectra of these galaxies arises in part as a result of the compression of emission-line gas clouds by the radio source shocks, decreasing the ionization parameter. The presence of extra (softer) ionizing photons associated with the shocks further influences the ionization state. Bicknell, Dopita & O'Dea (1997; see also Dopita & Sutherland 1996) have investigated the emission-line luminosity that can be generated by radio source shocks expanding through a single-phase ISM with a power-law

density gradient, $\rho(r) = \rho_0(r/r_0)^{-\delta}$. For $\delta = 2$, they show that the work done on the ISM by the expanding radio cocoon (PdV) is approximately half of the energy supplied by the radio jet; if the shock is fully radiative then a significant proportion of this energy is fed into emission-line luminosity. The luminosity of the [O III] 5007 emission-line can be estimated as

$$L([\mathrm{O\,III}]) \approx \frac{6}{8-\delta}\left(\frac{\kappa_{1.4}}{10^{-11}}\right)^{-1}\left(\frac{P_{1.4}}{10^{27}\,\mathrm{W\,Hz^{-1}}}\right)\times 10^{43}\,\mathrm{erg\,s^{-1}},$$

where $P_{1.4}$ is the monochromatic power of the radio source at 1.4 GHz, and $\kappa_{1.4}$ is the conversion factor from the energy flux of the jet to the monochromatic radio power at 1.4 GHz, which Bicknell et al. (1997) estimate to be of order $10^{-10.5}$. Adopting this value, taking the flux density of a typical $z \sim 1$ 3CR source at an observed frequency of 1.4 GHz to be 2 Jy, and assuming that the [O II] 3727/[O III] 5007 emission-line flux ratio is ~0.5 (McCarthy 1993), then for $\delta = 2$ the observed [O II] 3727 emission-line flux produced by the shocks is calculated to be $f([\mathrm{O\,II}]) \sim 3\times10^{-15}\,\mathrm{erg\,s^{-1}\,cm^{-2}}$. Of this, probably between a third and a half (that is, 1 to $1.5\times10^{-15}\,\mathrm{erg\,s^{-1}\,cm^{-2}}$) will fall within the projected sky area from which the spectrum was extracted. This predicted emission-line flux can be compared to the [O II] 3727 emission-line fluxes observed in the data (Table 1), which lie in the range ~0.5 to $5\times10^{-15}\,\mathrm{erg\,s^{-1}\,cm^{-2}}$ with the smaller radio sources typically having the higher values (see also Fig. 6). These results are completely consistent with a small (factors of 2 to 5) boosting of the emission-line luminosities of small sources as a result of the extra energy input from the shocks.

Once the radio source shocks have passed beyond the emission-line clouds, the shock-induced emission-line luminosity will fall. Under the simplest assumptions, once the jets pass beyond the confining ISM the pressure inside the cocoon will drain away, and the cocoon wall shocks will no longer be pressure driven (e.g. Dopita 1999). These shocks will pass into a momentum-conserving phase; their velocity will decrease roughly as $v_s \propto r^{-2}$, and so since the shock luminosity per unit area scales as v_s^3, the shock-induced emission-line luminosity will fall as r^{-4}. Although these assumptions are oversimplified, taking no account of confinement by an intracluster medium for example, it is clear that once the shock fronts have passed well beyond the emission-line regions, the contribution of ionizing photons produced by the shocks will decrease rapidly; this is in complete accord with the larger sources having photoionization-dominated emission-line regions.

4.3 The physical extent of the emission-line gas

The physical extent of the emission-line region of each galaxy along the slit direction was provided in Table 1. For comparison, the extent of the aligned optical (rest frame UV) emission has also been determined from the *HST* observations of Best et al. (1997); using the *HST* image taken through the filter at a rest frame wavelength of about 4000 Å, the angular distance over which optical emission was observed at greater than three times the rms sky noise level of the image was measured for each galaxy, and the corresponding 'optical sizes' are given in Table 1. These values can further be compared with these results of Best et al. (1998), who showed from near-infrared imaging that, underlying the aligned emission, the radio sources are hosted by giant elliptical galaxies with characteristic radii of typically 10 to 15 kpc.

The extent of the optical aligned emission does not exceed 25 kpc except in three cases: 3C 247, 3C 265 and 3C 368. For 3C 368, the *HST* 'continuum' image is actually dominated by a combination of line emission and the correspondingly luminous nebular continuum emission (see discussion in Section 4.5, below). The large extent of 3C 247 is also likely to be predominantly line emission, since it arises from a diffuse halo of emission exactly tracking that seen in a narrow-band [O II] 3727 image by McCarthy et al. (1995).

With the exception of 3C 265 (which, as discussed in Paper I, is an unusual source in many ways), it is therefore reasonable to say that the aligned continuum emission has an extent of only a couple of characteristic radii, and so lies within the body of the host galaxy. The situation with the emission-line gas is very different: this has a physical extent which can exceed 100 kpc, with a mean extent of over 60 kpc. The emission-line gas clearly extends well beyond the confines of the host galaxy. As was shown in Fig.7, there is also a difference in the physical extent of the line-emitting regions between large and small radio sources, with line emission at radii of 30 to 50 kpc generally only seen in small radio sources. Unless there is an intrinsic difference between the environments of the small and large radio sources, which seems unlikely given all of the correlations found, the emission-line gas clouds must also be present out to radii $\gtrsim$30 kpc in large radio sources, but this is not visible.

Again, the role of shocks can be considered to explain this. At these radii, the flux of ionizing photons from the active nucleus may be insufficient to produce an observable emission-line luminosity. As the radio source shocks pass through these regions, however, the gas density will be increased and, as discussed above, a large source of local ionizing photons will become available, pushing up the emission-line luminosity. Following the passage of the radio shocks and the consequent removal of the associated ionizing photons, this enhanced line emission will fade over time-scales much shorter than the radio source lifetime. Thus, luminous line emission is only seen from the clouds at radii 30 to 50 kpc at the time that the radio source shocks are passing through these regions. A direct consequence of this model is that for radio sources smaller than about 100 kpc a positive correlation between radio source size and emission-line region size should be observed, since line emission from the clouds at radii 30 to 50 kpc will not be seen until the radio source has advanced that far. Such a correlation has indeed been observed in the Lyα emission of radio galaxies with $z \gtrsim 2$ (van Ojik et al. 1997).

An interesting test of the model presented here could be carried out by taking high spatial resolution long-slit spectra of a sample of radio galaxies with radio sizes smaller than the size of the emission-line regions. The prediction is that within the region of the host galaxy occupied by the radio source, the radio source shocks will be important; the emission-line ratios will be consistent with shock ionization, and the gas kinematics will be distorted with broad velocity dispersions. Outside of this region, however, the gas clouds will not yet have been influenced by the radio source shocks and photoionization should dominate. A study with a similar principle has been carried out on the radio source 1243+036, a radio galaxy of radio size about 50 kpc at a redshift $z = 3.6$. Distorted Lyα velocity structures with large-velocity FWHM are seen within the radio source structure, but Lyα emission also extends beyond that to at least 75 kpc radius in an apparently rotating halo (van Ojik et al. 1996). Villar-Martín et al. (1999) have also found that the line emission of PKS 2250–41 ($z = 0.308$) is composed of distinct kinematic components: a low-ionization component with broad velocity width in the region of

the radio source structure, and a narrower high-ionization component which extends beyond the radio lobe. Carrying out studies such as these for a large sample of radio sources is important, because the velocity structures of the line emission in regions outside the radio shocks will directly show the initial motions of the emission-line clouds and can be used to determine whether these clouds are simply material associated with the formation of the galaxy which has been expelled into the IGM, or whether they have an external origin, brought in either by a galaxy merger or a cooling flow. It is difficult to distinguish between such scenarios in larger radio sources since information on the initial cloud velocities has been destroyed by the bow shock acceleration.

4.4 Evolution of the velocity structures

One significant issue remains to be explained in this picture, and that is how the velocity structures of the large radio sources are produced. The high gas velocities and velocity dispersions induced by the shocks in small radio sources are seen to evolve within the time-scale of a radio source lifetime, a few $\times 10^7$ yr, such that the emission-line clouds obtain an underlying velocity profile consistent with a rotating halo, albeit with a still-high velocity dispersion. Questions that need to be considered are whether this truly is rotation that is being seen, over what time-scale can the extreme shock-induced kinematics be damped down, and can a mean rotation profile be produced whilst the velocity dispersion remains so high?

Regarding the first question, given the single slit position and relatively low spatial resolution for the high-redshift radio galaxies, it cannot categorically be stated that the emission-line profiles of large radio sources are rotation profiles. The data are consistent, for example, with outflow along the radio axes, although in this case it is not clear why the velocity increases with radius (a structure more like that of 3C 324 – see Paper I – might be expected) while the velocity dispersion decreases with increasing source size. At low redshifts, however, much higher spatial resolution studies using multiple slit positions show clearly that the gas is in rotating structures (e.g. Baum et al. 1990). It therefore seems reasonable to assume that this may also be true at higher redshifts, and even if this is not the case, the questions noted above still need to be addressed for the low-redshift radio sources.

Three plausible mechanisms can be considered for the evolution in the velocities of the emission-line clouds over the radio source lifetime. The first is that the emission-line clouds settle back into stable orbits within the host galaxy through gravitational dynamics alone. The time-scale for this process is of the order of a few crossing times of the clouds, where for clouds moving with velocity $v_c \sim 500\,\mathrm{km\,s^{-1}}$ at a radius $r \sim 15$ kpc in the galaxy, the crossing time is $t_c \sim 2r/v \sim 6 \times 10^7$ yr. This time-scale is longer than the radio source lifetime, and so gravity alone cannot give rise to the observed evolution in the emission-line structures.

A second possibility concerns the deceleration of emission-line clouds moving with respect to the interstellar medium, as a result of ram-pressure. This works through the same process as the acceleration discussed in Section 4.2. As the emission-line clouds move through the intercloud gas, those clouds moving with the largest velocities sweep up the greatest mass of intercloud gas, and so are decelerated most strongly. This process will decrease the width of the cloud velocity distribution.

Simulations have been carried out, as detailed in Appendix A, to investigate the time-scale over which the mean velocity of an ensemble of emission-line clouds (with an initial velocity distribution similar to that seen in small radio sources) evolves to that of the IGM in which the clouds are moving, and the time-scale over which the dispersion of the velocity distribution is decreased. It is found that the peak of the velocity distribution evolves to that of the gas in which it is moving considerably more quickly than the velocity width decreases. Both time-scales depend upon the typical cloud size and the ratio of the cloud density to that of the intercloud medium within the radio cocoon, and for reasonable assumptions the time-scale for decrease of the velocity widths is comparable to the radio source lifetime (see Appendix A for details).

Therefore, if a population of emission-line clouds were placed within the rotating ISM of a galaxy, a mean rotation profile for the emission-line clouds could be recovered whilst the FWHM of the emission-lines remained large, as is observed in the radio galaxies. The problem with this model, however, is that the radio bow shock sweeps up essentially all of the intercloud gas, with little mixing through the contact discontinuity (e.g. Norman et al. 1982). The radio cocoon is filled primarily with material supplied by the radio jets, and so there is essentially no gas left following a rotation profile. Such gas would have to be resupplied to the ISM, for example by supernovae and stellar winds from stars in rotational orbits, but it is very unlikely that enough gas could be supplied in this manner. Alternatively, the cocoon material supplied by the radio jets would itself have to be in rotational motion, perhaps through angular momentum transfer from the rotating IGM to the radio source as the bow shocks advance. To summarize: although this mechanism can decrease the velocity widths of the gas, it is not clear whether a rotation profile can be re-established quickly enough.

The third possibility considers the evolution of the population of radiating clouds through a combination of galaxy rotation and cloud shredding. Klein, McKee & Colella (1994) showed that in the aftermath of a bow shock, emission-line clouds may be susceptible to shredding as a result of growing Kelvin–Helmholtz and Rayleigh–Taylor instabilities on their surfaces. The clouds could be shredded over a time-scale of a few 'cloud crushing times', $t_{cc} \sim \chi^{1/2} r_c / v_b$, where χ is the density ratio of the cloud to the surrounding medium inside the cocoon, r_c is the post-shock cloud radius, and v_b is the velocity of the bow shock through the IGM. Kaiser, Schoenmakers & Röttgering (1999) considered such cloud disruption as a way to resupply material to the radio cocoon in order to explain how a secondary hotspot could be formed in the newly discovered class of double–double radio galaxies (e.g. Schoenmakers et al. 1999); they derived a value of $t_{cc} \sim 5 \times 10^6 (r_c/\mathrm{pc})$ yr.

The cloud-shredding time is shortest for the smallest emission-line clouds; clouds smaller than about a parsec will be shredded on time-scales shorter than the radio source lifetime. These small clouds were the most rapidly accelerated (see equation 1) and so are responsible for producing much of the high velocity dispersions and distorted velocity structures. If these high-velocity small clouds are destroyed, then the line emission will become dominated by the remaining more massive clouds, which were less accelerated by the radio source shocks, have a lower velocity dispersion, and may still maintain the vestiges of a rotation profile.

Equation (1) further shows that the velocity acquired by the warm clouds is proportional to the velocity of the bow shock. In directions perpendicular to the radio axis, the bow shock velocity

is lower by a factor of the aspect ratio of the cocoon (typically between about 1.5 and 6, e.g. Leahy, Muxlow & Stephens 1989), and so the warm clouds in these directions will be less accelerated. In small radio sources, these clouds will not be very luminous since they lie away from the strongest radio source shocks and outside of the cone of photoionizing radiation from the partially obscured AGN; the emission will be dominated by the higher velocity clouds along the radio jet direction. Over a rotation timescale ($\sim 10^7$ yr), however, these low-velocity clouds may be brought within the ionization cone of the AGN, become ionized, and contribute significantly to the emission-line luminosity. Likewise, clouds in small radius orbits around the AGN will acquire lower velocities, since the distance between the bow shock and the contact discontinuity is less and so the period of acceleration is shorter. Thus the rotation profile may re-establish itself from the central regions of the galaxy outwards.

By these two mechanisms of shredding and mixing of the cloud populations, the observed population of emission-line clouds will evolve such that, in large radio sources, an increasing percentage of the emission will arise from clouds which were less accelerated by the bow shock and so the rotation profile will be gradually recovered. The cloud-shredding model has a further advantage that if some fraction of the clouds is destroyed in large radio sources, then the emission-line luminosity will decrease with increasing radio size, as is observed. The one drawback of this model is that it is surprising that the distinction between radio sources showing rotation profiles and those with distorted profiles is so sharp. Note also that if this scenario is the correct one, then the emission-line clouds must lie in rotating orbits prior to the radio source activity, providing some information as to their origin.

In conclusion, the observation of emission-line clouds in rotating haloes around large radio galaxies is not trivial to explain, given the large influence of the radio source bow shocks passing through the medium. Gravitational effects alone cannot be responsible for re-establishing rotation profiles, but a combination of cloud shredding and cloud mixing, maybe with some help from ram-pressure deceleration, could reproduce the effect.

4.5 Implications for the alignment effect

In 1987, McCarthy et al. and Chambers et al. demonstrated that the optical–UV emission of radio galaxies with redshifts $z \gtrsim 0.6$ has a strong tendency to be elongated and aligned along the direction of the radio source. *HST* images of a sample of 28 of these radio galaxies (Best et al. 1997) have demonstrated that the form of this so-called 'alignment effect' varies strongly from galaxy to galaxy, and in particular appears to evolve with increasing size of the radio source (Best et al. 1996). Small radio sources show a number of intense blue knots tightly aligned along the direction of the radio jet, whilst larger sources generally have more diffuse optical–UV morphologies. Given the strong similarity between this radio size evolution of the continuum alignment effect and the evolution of the emission-line gas properties, it is instructive to examine the role of the radio source shocks and the emission-line clouds in giving rise to continuum emission.

One direct connection is the nebular continuum emission from the warm emission-line gas clouds (Dickson et al. 1995), that is, free–free emission, free–bound recombination, two-photon continuum and the Balmer forest lines. The flux density of this emission is directly connected to the flux of the Hβ emission-line. The very luminous line emission seen in the spectra of these powerful radio galaxies (e.g. Paper I) thus implies that nebular continuum emission is likely to make a significant contribution to their UV flux density. Indeed, 3C 368 was one of the original three radio galaxies studied by Dickson et al. (1995), and they found a nebular continuum contribution in the northern knots as high as 60 per cent of the total continuum emission at rest frame wavelengths just below the 3646 Å Balmer break (see also Stockton et al. 1996). As can be seen from Table 1, 3C 368 is a somewhat extreme case and the contribution for more typical galaxies will be somewhat lower, but still of great significance. In Section 3 (above) it was shown that the luminosity of the emission-lines correlated inversely with the size of the radio source (Fig. 6); therefore, the strength of nebular continuum emission will decrease with increasing radio source size, and in small sources will be found predominantly along the radio jet tracing the strongest radio source shocks. This reflects exactly the observed evolution of the continuum alignment effect.

A second alignment effect hypothesis involving the emission-line clouds is that star formation is induced by the passage of the radio jet, as a result of the radio source shocks compressing gas clouds and pushing them over the Jeans limit (e.g. Rees 1989; Begelman & Cioffi 1989; De Young 1989). It should be noted that it is the most massive clouds which would collapse to form the stars, and these are distinct from the smallest clouds which are the most likely to be destroyed by the bow shock. In regions which might be star-forming, $\lesssim 10^6$ yr behind the bow shock, the only clouds which will already have been destroyed by instabilities on their surface are those of size $r_c \lesssim 0.1$ pc (see Section 4.3); for a mean cloud density of 100 cm^{-3}, this corresponds to a total cloud mass of less than $10^{-2}\,M_\odot$, not massive enough to have formed a star anyway.

As discussed by Best et al. (1996), the jet-induced star formation mechanism can also account directly for the evolution of the optical–UV morphology with radio size: the mass of stars required to produce the excess optical–UV emission is only a few $\times 10^8\,M_\odot$ (Lilly & Longair 1984; Dunlop et al. 1989), well below 1 per cent of the stellar mass of the galaxy, and since the starburst luminosity drops rapidly with age they become indistinguishable from the evolved star population over a timescale of a few $\times 10^7$ yr. On the negative side, no direct evidence for young stars in these radio galaxies was found in our spectra (cf. 4C41.17 at higher redshift, $z = 3.8$; Dey et al. 1997), although the clearest features of young stellar populations fall outside the observed wavelength ranges.

Another important continuum alignment model is the scattering of light from a hidden quasar nucleus by electrons (Fabian 1989) or dust (e.g. Tadhunter et al. 1989a; di Serego Alighieri et al. 1989). Strong support for this model comes from the observation that the optical emission of some distant radio galaxies is polarized at the ~ 10 per cent level with the electric vector oriented perpendicular to the radio axis (e.g. Cimatti et al. 1996 and references therein), and the detection of broad permitted lines in polarized light (Dey & Spinrad 1996; Cimatti et al. 1996; Tran et al. 1998): clearly some fraction of the excess optical–UV emission must be associated with this mechanism. However, the lack of polarized emission from some sources (e.g. 3C 368, van Breugel 1996; see also Tadhunter et al. 1997) dictates that this is not universal; even for 3C 324 where the polarization percentage is high, only a fraction $\lesssim$30–50 per cent of the optical–UV emission is associated with the scattered component (Cimatti et al.

1996). A problem for scattering models is that, in the simplest picture, a biconical emission region is expected for the scattered light, rather than the knotty strings of emission observed to lie along the radio jet. However, in light of jet-shock models, this could be explained by extra scattering particles being made available along the radio jet axis, either as dust grains being produced in jet-induced star forming regions, or by radio source shocks disrupting optically thick clouds along the radio-jet direction and exposing previously hidden dust grains (Bremer, Fabian & Crawford 1997).

In conclusion, radio source shocks will play a key role in producing the observed morphology and radio size evolution of the continuum alignment effect. Nebular continuum emission will be enhanced in small radio sources, some gas clouds may be induced to collapse and form stars, and extra scattering particles associated either with any star formation or the disruption of gas clouds could enhance the scattered component.

5 CONCLUSIONS

The main conclusions of this work can be summarized as follows.

(i) Small radio sources show a lower ionization state than large radio sources. The emission-line ratios of radio sources with linear sizes $\lesssim$120 kpc are consistent with the gas being ionized by photons produced by the shocks associated with the radio source. The emission-line luminosities of the small sources are boosted by a small factor ($\sim$2–5) relative to large sources, in accord with them receiving an extra source of ionizing photons from the shock.

(ii) Small radio sources have very distorted velocity profiles, large velocity widths, and emission-line regions covering a larger spatial extent than those of large sources; the latter have much smoother velocity profiles which appear to be dominated by gravitation. These properties are fully explained in terms of the passage of the shocks associated with the radio source.

(iii) A strong correlation is found between the ionization state of the gas and its kinematical properties, indicating that the two are fundamentally connected.

(iv) These correlations, originally derived for the sample of $z \sim 1$ radio galaxies studied in Paper I, are shown also to hold for a sample of FR II radio galaxies with redshifts $z \lesssim 0.2$.

(v) The similarity of the evolution of the emission-line gas properties with radio size to that of the continuum alignment effect makes a strong case for the continuum alignment effect also having a large dependence upon radio source shocks.

(vi) The continuum alignment effect is generally confined to within the extent of the host galaxy, but line emission is observed over a considerably larger spatial extent.

ACKNOWLEDGMENTS

The William Herschel Telescope is operated on the island of La Palma by the Isaac Newton Group in the Spanish Observatorio del Roches de los Muchachos of the Instituto de Astrofísica de Canarias. This work was supported in part by the Formation and Evolution of Galaxies network set up by the European Commission under contract ERB FMRX-CT96-086 of its TMR programme. We are grateful to Mark Allen for supplying the output of the MAPPINGS II photoionization models in digitized form, and Hy Spinrad for providing the Neon line ratios for 3C 217 and 3C 340. We thank Matt Lehnert, Arno Schoenmakers and Christian Kaiser for useful discussions, and the referee, Mike Dopita, for his careful consideration of the original manuscript and a number of useful suggestions.

REFERENCES

Allen M. G., Dopita M. A., Tsvetanov Z. I., 1998, ApJ, 493, 571
Antonucci R., 1993, ARA&A, 31, 473
Baldwin J. A., Phillips M. M., Terlevich R., 1981, PASP, 93, 5
Barthel P. D., 1989, ApJ, 336, 606
Baum S. A., Heckman T. M., van Breugel W. J. M., 1990, ApJS, 74, 389
Baum S. A., Heckman T. M., van Breugel W. J. M., 1992, ApJ, 389, 208
Baum S. A., Zirbel E. L., O'Dea C. P., 1995, ApJ, 451, 88
Begelman M. C., Cioffi D. F., 1989, ApJ, 345, L21
Best P. N., Longair M. S., Röttgering H. J. A., 1996, MNRAS, 280, L9
Best P. N., Longair M. S., Röttgering H. J. A., 1997, MNRAS, 292, 758
Best P. N., Longair M. S., Röttgering H. J. A., 1998, MNRAS, 295, 549
Best P. N., Röttgering H. J. A., Longair M. S., 1999, MNRAS, 311, 1 (Paper I, this issue)
Bicknell G. V., Dopita M. A., O'Dea C. P., 1997, ApJ, 485, 112
Binette L., Wilson A. S., Storchi-Bergmann T., 1996, A&A, 312, 365
Bremer M. N., Fabian A. C., Crawford C. S., 1997, MNRAS, 284, 213
Chambers K. C., Miley G. K., van Breugel W. J. M., 1987, Nat, 329, 604
Cimatti A., Dey A., van Breugel W., Antonucci R., Spinrad H., 1996, ApJ, 465, 145
Clarke D. A., Burns J. O., 1991, ApJ, 369, 308
Clark N. E., Tadhunter C. N., Morganti R., Killeen N. E. B., Fosbury R. A. E., Hook R. N., Siebert J., Shaw M. A., 1997, MNRAS, 286, 558
Clark N. E., Axon D. J., Tadhunter C. N., Robinson A., O'Brien P., 1998, ApJ, 494, 546
de Koff S. et al., 2000, ApJS, in press
De Young D. S., 1989, ApJ, 342, L59
Dey A., Spinrad H., 1996, ApJ, 459, 133
Dey A., van Breugel W. J. M., Vacca W. D., Antonucci R., 1997, ApJ, 490, 698
di Serego Alighieri S., Fosbury R. A. E., Quinn P. J., Tadhunter C. N., 1989, Nat, 341, 307
Dickson R., Tadhunter C., Shaw M., Clark N., Morganti R., 1995, MNRAS, 273, L29
Dopita M. A., 1999, in Berry D., da Costa A., Dyson J., eds, Astrophysical Dynamics. Astrophysics and Space Science, in press
Dopita M. A., Sutherland R. S., 1996, ApJS, 102, 161
Dunlop J. S., Guiderdoni B., Rocca-Volmerange B., Peacock J., Longair M., 1989, MNRAS, 240, 257
Fabian A. C., 1989, MNRAS, 238, 41P
Fanaroff B. L., 1974, MNRAS, 167, 31P(FR)
Hammer F., Le Fèvre O., Proust D., 1991, ApJ, 374, 91
Heckman T. M., Baum S. A., van Breugel W. J. M., McCarthy P. J., 1989, ApJ, 338, 48
Hill G. J., Lilly S. J., 1991, ApJ, 367, 1
Kaiser C. R., Alexander P., 1997, MNRAS, 286, 215
Kaiser C. R., Alexander P., 1999, MNRAS, 305, 707
Kaiser C. R., Schoenmakers A. P., Röttgering H. J. A., 1999, MNRAS, in press
Klein R. I., McKee C. F., Colella P., 1994, ApJ, 420, 213
Lacy M., Rawlings S., 1994, MNRAS, 270, 431
Lacy M., Rawlings S., Blundell K. M., Ridgway S. E., 1998, MNRAS, 298, 966
Laing R. A., Riley J. M., Longair M. S., 1983, MNRAS, 204, 151
Leahy J. P., Muxlow T. W. B., Stephens P. W., 1989, MNRAS, 239, 401
Ledlow M. J., Owen F. N., 1996, AJ, 112, 9
Lilly S. J., Longair M. S., 1984, MNRAS, 211, 833
Liu R., Pooley G., Riley J. M., 1992, MNRAS, 257, 545
Longair M. S., Best P. N., Röttgering H. J. A., 1995, MNRAS, 275, L47
McCarthy P. J., 1993, ARA&A, 31, 639
McCarthy P. J., van Breugel W. J. M., Spinrad H., Djorgovski S., 1987, ApJ, 321, L29
McCarthy P. J., Spinrad H., van Breugel W. J. M., 1995, ApJS, 99, 27

McCarthy P. J., Baum S. A., Spinrad H., 1996, ApJS, 106, 281
Norman M. L., Smarr L., Winkler K.-H. A., Smith M. D., 1982, A&A, 113, 285
Owsianik I., Conway J. E., 1998, A&A, 69, 337
Owsianik I., Conway J. E., Polatidis A. G., 1998, A&A, 336, L370
Rawlings S., Lacy M., Sivia D. S., Eales S. A., 1995, MNRAS, 274, 428
Rees M. J., 1989, MNRAS, 239, 1P
Reynolds C. S., Di Matteo T., Fabian A. C., Hwang U., Canizares C. R., 1996, MNRAS, 283, L111
Robinson A., Binette L., Fosbury R. A. E., Tadhunter C. N., 1987, MNRAS, 227, 97
Schoenmakers A. P., de Bruyn A. G., Röttgering H. J. A., van der Laan H., Kaiser C. R., 1999, MNRAS, in press
Smith H. E., Junkkarinen V. T., Spinrad H., Grueff G., Vigotti M., 1979, ApJ, 231, 307
Spinrad H., 1982, PASP, 94, 397
Stockton A., Ridgway S. E., Kellogg M., 1996, AJ, 112, 902
Sutherland R. S., Bicknell G. V., Dopita M. A., 1993, ApJ, 414, 510
Tadhunter C. N., 1991, MNRAS, 251, 46P
Tadhunter C. N., Fosbury R. A. E., di Serego Alighieri S., 1989a, in Maraschi L., Maccacaro T., Ulrich M.-H., eds, BL Lac Objects. Springer Verlag, Berlin, p. 79
Tadhunter C. N., Fosbury R. A. E., Quinn P. J., 1989b, MNRAS, 240, 225
Tadhunter C., Dickson R., Morganti R., Villar-Martín M., 1997, in Clements D. L., Pérez-Fournon I., eds, Quasar Hosts. Springer-Verlag, Berlin, p. 311
Tadhunter C. N., Morganti R., Robinson A., Dickson R. D., Villar-Martín M., Fosbury R. A. E., 1998, MNRAS, 298, 1035
Tran H. D., Cohen M. H., Ogle P. M., Goodrich R. W., di Serego Alighieri S., 1998, ApJ, 500, 660
van Breugel W. J. M., 1996, in Ekers R., Fanti C., Padrielli L., IAU Symp. 175: Extragalactic radio sources. Kluwer, Dordrecht, p. 577
van Breugel W. J. M., Miley G. K., Heckman T. M., 1984, AJ, 89, 5
van Ojik R., Röttgering H. J. A., Carilli C., Miley G. K., Bremer M. N., Macchetto F., 1996, A&A, 313, 25
van Ojik R., Röttgering H. J. A., Miley G. K., Hunstead R., 1997, A&A, 317, 358
Viegas S. M., Prieto A., 1992, MNRAS, 258, 483
Villar-Martín M., Tadhunter C., Clark N., 1997, A&A, 323, 21
Villar-Martín M., Tadhunter C., Morganti R., Axon D., Koekemoer A., 1999, MNRAS, 307, 24
Zirbel E. L., Baum S. A., 1995, ApJ, 448, 521

APPENDIX A: DECELERATION OF EMISSION-LINE CLOUDS MOVING THROUGH THE IGM

Consider a spherical cloud of emission-line gas with number density n_c and radius r_c travelling at velocity v_c through gas of number density n_g and velocity v_g. In a time dt a mass of gas of approximately $\pi r_c^2 n_g m_p (v_c - v_g)\,\mathrm{d}t$, where m_p is the proton mass, is displaced by the cloud and accelerated from velocity v_g to velocity v_c. The momentum of the cloud is correspondingly decreased:

$$\frac{4}{3}\pi r_c^3 n_c m_p\,\mathrm{d}v_c = \pi r_c^2 n_g m_p (v_c - v_g)^2\,\mathrm{d}t.$$

Defining t_0 as $t_0 = 4n_c r_0/3n_g$, where r_0 is a typical cloud radius, then

$$\mathrm{d}v_c = \frac{(v_c - v_g)^2}{r_c/r_0}\frac{\mathrm{d}t}{t_0}.$$

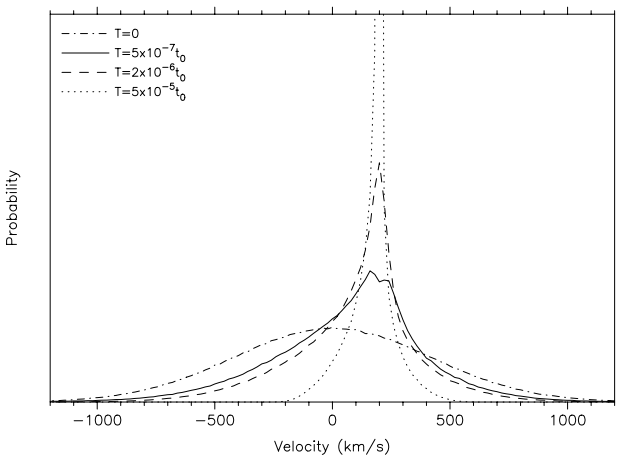

Figure A1. Modelling the evolution of the emission-line cloud velocity distribution within gas moving at 200 km s^{-1}.

Using this equation, it is possible to follow the evolution of an ensemble of such emission-line clouds. For simplicity, the distribution of emission-line cloud radii was chosen to be flat in logarithm space over a factor of 1000 range centred on r_0, that is, P[log (r_c)] is constant in the range $-1.5 \leq \log(r_c/r_0) \leq 1.5$, and 0 outside that range. The initial velocity distribution of the clouds was set to follow a Gaussian distribution with a mean velocity of zero and a FWHM of 1000 km s^{-1}, chosen to represent the velocity dispersion observed in small radio sources. A Monte Carlo simulation was then used to follow the evolution of the velocity distribution of the cloud population in gas moving with velocity +200 km s^{-1}, typical of the relative velocity offsets seen in the galaxy profiles; the results are shown in Fig. A1.

It can be seen that the peak of the velocity distribution of the cloud population evolves rapidly to that of the gas in which it is moving; the width of the velocity distribution becomes progressively narrower but over a much longer time-scale. The resulting velocity distribution is no longer Gaussian, but can be approximated as a Gaussian distribution plus extended broad wings (the slight dip at 200 km s^{-1} for the first plotted time interval should be ignored; it arises only because of the simplicity of the model in which a cloud with an initial velocity close to 200 km s^{-1} will decelerate very slowly).

The time-scale over which the FWHM of the emission-line clouds decreases to that observed in large radio sources (a few hundred km s^{-1}) can be used to test the plausibility of this model. This time interval is $T \approx 5 \times 10^{-7} t_0$ (the solid line on Fig. A1), where $t_0 = 4n_c r_0/3n_g$. Taking $T \sim 3 \times 10^7$ yr as an appropriate age for radio sources a few hundred kpc in size, and assuming pre-shock density ratio $n_c/n_g \sim 10^4$ with the IGM density decreased a further factor Δ by the bow shock, this gives $(r_0/\mathrm{pc})\Delta \approx 5$. For $\Delta \approx 40$ (e.g. Clarke & Burns 1991), the median cloud size would be about about 0.15 parsec; although small, this is certainly plausible given the simplicity of the assumptions.

This paper has been typeset from a TEX/LATEX file prepared by the author.